A large-area near-infrared emission line survey for star forming galaxies at $z = 2.1$–$2.4^\star$

P.P. van der Werf[1]**, A.F.M. Moorwood**[2]**, and M.N. Bremer**[1,3,$\star\star$]

[1] Leiden Observatory, P.O. Box 9513, 2300 RA Leiden, The Netherlands
[2] European Southern Observatory, Karl-Schwarzschild-Strasse 2, 85748 Garching bei München, Germany
[3] Institut d'Astrophysique de Paris, 98bis Blvd. Arago, 75014 Paris, France

Abstract. We present a large-area survey for Hα emission at redshifts from 2.1 to 2.4, using a combination of deep narrow-band and broad-band imaging in the near-infrared K-band. Our survey covers half the comoving volume of the widest available survey to date, but goes considerably deeper. We target volumes containing known damped Lyα systems and radio galaxies as well as random fields. We detect (in addition to the two radio galaxies and one known active galaxy) four Hα emission objects, with implied star formation rates of 44 to 73 h_{75}^{-2} M$_\odot$ yr^{-1} for $q_0 = 0.1$ and no extinction correction. It is argued that these objects are most likely star forming galaxies at $z = 2.1$–2.4. The density of such sources in fields targeted at absorption line systems is found to be much higher than that in the vicinity of radio galaxies or quasars or in the general field at these redshifts. We discuss the properties of our detected sources and target fields, and suggest how future surveys of this type can be used to derive the cosmic star formation history.

Key words: galaxies: evolution – galaxies: starburst

1. Introduction

The star formation properties of the universe at high redshift are at the focus of current observational research in cosmology. Moderate redshift surveys consistently indicate a star formation density (SFD) $\dot\rho_*$ that strongly increases with redshift out to $z \sim 1$ (Lilly et al. 1996). The SFD at $z > 1$ is however a hotly debated issue. Estimates based on surveys for Lyman break galaxies, not corrected for extinction, indicate an SFD (based on rest-frame UV radiation) that strongly decreases with redshift at $z > 1$ (e.g., Madau et al. 1996), wheras submillimetre surveys (e.g., Hughes et al. 1998; Blain et al. 1999) indicate a much more constant SFD at these redshifts. While inclusion of realistic extinction values (e.g., Pettini et al. 1998; Steidel et al.

1999) in the UV-based determinations make these results more consistent, these complications can be largely avoided by using a star formation tracer that is relatively insensitive to extinction, and by using the same tracer at all redshifts. The Hα line is the natural choice for this tracer, since as a result of the development of large area, high quality near-infrared arrays, this line can now be observed in the J, H and K-bands, where redshifts of approximately 1, 1.5 and 2.2 respectively, are accessible.

Traditionally, surveys for high-z star forming galaxies have targeted the Lyα line, which moves into the optical regime for $z = 1.9$–7.0. However, since Lyα is resonantly scattered, even very small quantities of dust will effectively suppress the line (Charlot & Fall 1991, 1993; Chen & Neufeld 1994). Indeed, despite painstaking efforts, wide-field, shallow Lyα surveys have not revealed a population of high-z starburst galaxies (see Thompson & Djorgovski 1995 for a compilation of the available limits). The recent spectroscopic observations of star forming $z > 3$ galaxies selected by the UV dropout technique (Steidel et al. 1996) confirm that Lyα is not a good tracer of star formation in high-z galaxies. The galaxies observed by Steidel et al. (1996) form stars at rates of ~ 10 M$_\odot$ yr^{-1} as derived from their restframe UV properties (uncorrected for extinction), but Lyα is absent (or in *absorption*) in more than 50% of the cases, while in most of the remaining objects the line is faint. Thus, while Lyα searches can be used to find *some* high-z star forming galaxies (e.g., Macchetto et al. 1993; Giavalisco et al. 1994; Hu & McMahon 1996; Hu et al. 1998; Cowie & Hu 1998), such surveys will miss a large fraction of these galaxies, and cannot provide reliable star formation rates (SFRs) $\dot M_*$ for the galaxies that are detected.

This complication is avoided by searching for Hα emission in stead of Lyα. The Hα line is not resonantly scattered and thus much less sensitive to the effects of small amounts of dust. In addition, the broad-band extinction at Hα (6563 Å) is much less than that at Lyα (1215 Å), $A_{\mathrm{Ly}\alpha}/A_{\mathrm{H}\alpha} = 4.28$ for the extinction curve used by Cardelli et al. (1989). Although the extinction at the wavelength of Hα is still large in starburst galaxies, the typical Hα extinction in local spiral galaxies is only $1^{\mathrm{m}}\!.1$ (Kennicutt 1983 and references therein). Indeed, recent Hα observations by Glazebrook et al. (1999) of a sample of $z \sim 1$ galaxies indicate SFRs at least three times higher than the UV-

estimated values. While measurements in the rest-frame UV-continuum can be approximately corrected for extinction using the slope of the spectrum in this region, leading to an average luminosity-weighted correction of a factor of 5.4 at 1600 Å in the rest frame (Meurer et al. 1999), Hα measurements can be extinction-corrected using measurements of the Balmer decrement. A recent comparison of star formation tracers (including stellar continuum emission as well as nebular lines) by Charlot (1999) confirms that Hα is the most robust star formation tracer for a given inital mass function (IMF). On the other hand, the IMF is in practice unknown, and since the Hα emission probes only the very top end of the IMF, the extrapolation to a total SFR is more uncertain for Hα than for other tracers (Glazebrook et al. 1999; Afonso et al. 2000). In summary, determinations of the cosmic SFD based on Hα and on the rest-frame UV continuum are complementary, and the combination of these may help to address effects of extinction and the assumed initial mass function on the results.

Since the background in the near-IR windows shortward of about 2.2 μm is dominated by OH emission lines, the narrow-band survey technique is the ideal approach in this spectral region (see Djorgovski 1992 for a comparison of various survey strategies). This technique involves deep imaging in a suitable narrow-band filter, complemented with broad-band imaging; sources with excess flux in the narrow-band filter are emission line candidates in a redshift interval determined by the narrow-band filter passband. This strategy has been analyzed in detail by Mannucci & Beckwith (1995). Narrow-band surveys of Hα emission at $z > 2$ have been presented by Thompson et al. (1994), Pahre & Djorgovski (1995), Bunker et al. (1995), Collins et al. (1996) and Thompson et al. (1996), but these surveys were either not sufficiently wide or sufficiently deep to find star forming galaxies (with the exception of one object reported by Beckwith et al. 1998). In contrast, an extensive Hα survey targeted at volumes containing Lyα and metal-line absorbers by Mannucci et al. (1998) resulted in the detection of a large number of objects. A significant number of detections was also found in a deep Hα survey by Teplitz et al. (1998) on a small (in total less than 12 $\square'$) region targeted at metal line absorption systems and environments of known quasars.

In this paper we describe a new survey for Hα emission at $z > 2$, covering about 50% of the volume of the widest survey to date (that by Thompson et al. 1996), but probing new parameter space by going considerably deeper. In addition, we target the environments of damped Lyα systems and radio galaxies as well as blank fields. In total, seven emission line objects are detected, including the two known radio galaxies. Our observations and reduction procedure are described in Sect. 2. Results are presented and discussed in Sects. 3 and 4. Our conclusions are summarized in Sect. 5. Throughout this paper we write the Hubble constant as $H_0 = 75 \, h_{75}$ km s^{-1} Mpc^{-1}.

2. Observations and reduction

We used the near-IR camera IRAC2B (Moorwood et al. 1992) at the ESO/MPI 2.2 m telescope at La Silla, Chile, during ob-

Table 1. Parameters of the survey fields

target field	z range (for Hα)	area [$\square'$]	3σ flux limit [erg s^{-1} cm^{-2}]	notes
Damped Lyα *fields:*				
UM 196	2.11–2.16	6.09	$1.4 \cdot 10^{-16}$	a
PHL 957	2.29–2.35	6.36	$1.7 \cdot 10^{-16}$	a
PKS 0528$-$250	2.11–2.16	6.03	$1.6 \cdot 10^{-16}$	a
Radio galaxy fields:				
TX 0200+015	2.19–2.26	6.37	$1.0 \cdot 10^{-16}$	b
TX 0211$-$122	2.29–2.35	6.26	$1.2 \cdot 10^{-16}$	b
Blank fields:				
Q0000$-$2619	2.29–2.35	6.19	$2.0 \cdot 10^{-16}$	c
Q0000$-$2619	2.34–2.44	6.21	$4.8 \cdot 10^{-16}$	c,d
TX 0211$-$122	2.34–2.44	6.13	$3.1 \cdot 10^{-16}$	c
MRC 0529$-$549	2.29–2.35	6.23	$1.4 \cdot 10^{-16}$	c

[a] contains a damped Lyα system with redshift within the range for Hα
[b] contains a radio galaxy with redshift within the range for Hα
[c] no object within the targeted redshift range for Hα known in this field
[d] contains [O III] 5007 Å at the redshift of a $z_{\mathrm{abs}} = 3.39$ damped Lyα system in this field, but since no line emitters were detected, analysed here for Hα

serving runs in September and October 1994 and August and September 1995. The detector was a 256×256 HgCdTe Rockwell NICMOS3 array. In order to optimize area coverage, the camera was for most targets used with a pixel scale of $0''.72$. Taking into account vignetting at the corners, this setup provides a useful field of view of $\approx 6.6 \, \square'$. Integration time was built up by shifting the field every few minutes, in a quasi-random pattern of $\sim 10''$ steps. This "dithering" method allows extremely accurate flatfielding and skysubtraction using "superflats" constructed directly from the data (e.g., Devillard et al. 1999). Total integration times varied from 8 to 13 hours in the typically 1.5–2% narrow-band filters containing Hα at a particular redshift interval and 4 to 6 hours in K'. Our survey fields included fields of known damped Lyα systems and high-z radio galaxies as well as "blank" fields (i.e., fields without known objects at the redshift that would bring Hα into the narrow-band filter). Parameters are summarized in Table 1. The flux scale was derived from observations of K-band standard stars during photometric nights, transformed to the K' scale using the expression

$$K' - K = 0.20 \, (H - K) \qquad (1)$$

(Wainscoat & Cowie 1992). Data obtained on non-photometric nights were reduced to the same flux scale. Individual frames were processed by subtracting the dark current, interpolating hot and cold pixels at fixed positions, and blanking vignetted areas. Subsequently flatfields were constructed by median filtering the stacked data frames; these flatfields were used both for flatfielding and for sky subtraction. After flux calibration the frames were converted to a common origin using the positions of bright objects as reference, and shifting frames only by integral pixels, in order not to introduce correlations between neighbouring pixels. Field edges with increased noise due to non-uniform coverage were discarded. Parameters of the result-
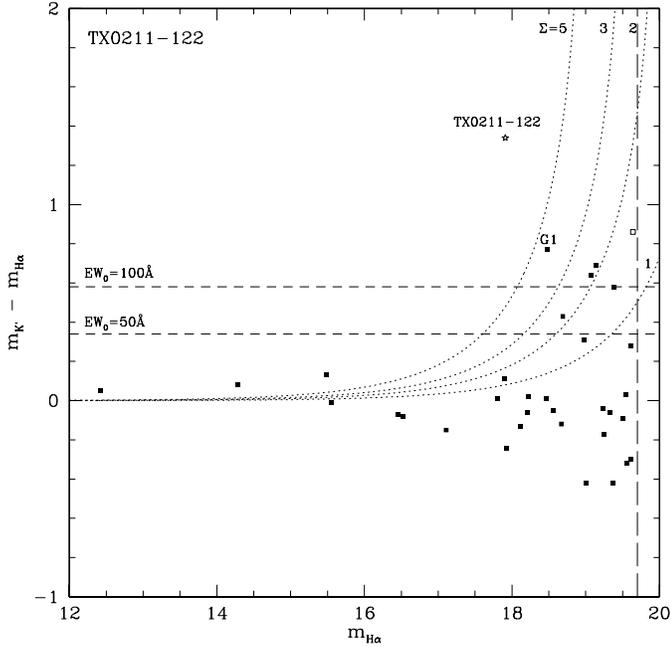
Fig. 1. Colour-magnitude diagram constructed from narrow-band ($m_{\mathrm{H}\alpha}$) and broad-band magnitudes ($m_{\mathrm{K}'}$) for the field centred on the $z = 2.336$ radio galaxy TX 0211$-$122 (Van Ojik et al. 1994) targeted at Hα for $z = 2.29$–2.35. Dotted curves indicate loci of constant "significance" Σ (see text). Dashed horizontal lines denote the rest-frame line equivalent widths indicated by EW$_0$. The dashed vertical line is the 3σ detection limit in the narrow-band frame. Open symbols denote sources only detected in the narrow-band frame and can thus be shifted upwards. The radio galaxy (denoted by a star) and the emission line object G1 are indicated.

ing coadded fields are listed in Table 1. The total area covered is $55.9 \,\square'$, the total comoving volume sampled for Hα emission is $8.8 \cdot 10^3 \, h_{75}^{-3}$ Mpc^3 for $q_0 = 0.1$, or $2.9 \cdot 10^3 \, h_{75}^{-3}$ Mpc^3 for $q_0 = 0.5$, which is about 50% of the volume of the widest survey to date (the survey by Thompson et al. 1996). However, with an area-weighted 3σ point-source sensitivity in the narrow-band frames of $2.0 \cdot 10^{-16}$ erg s^{-1} cm^{-2}, our survey is considerably deeper.

We used SExtractor (Bertin & Arnouts 1996) to measure the magnitudes of individual sources in the narrow and broad-band frames, in identical apertures of 1.5 times the seeing, for an optimum S/N ratio (Howell 1989). For the two radio galaxies, larger apertures were used in order to include diffuse extended emission. The resulting magnitudes were used to construct colour-magnitude diagrams for each field.

3. Results

For all objects with a narrow-band flux excess we computed the significance Σ of the excess, as defined by Bunker et al. (1995). This significance corresponds to a S/N ratio of the narrow-band excess, taking into account the uncertainties both in the narrow-band and in the broad-band frame magnitudes. Only objects with $\Sigma > 3$ and an Hα rest-frame equivalent width EW$_0 > 100$ Å (in order to select against bright sources with sloping continuum

in the K-band, which would show up as highly significant candidates but with a low EW$_0$) were accepted as reliable emission-line objects. This cutoff necessarily introduces incompleteness, since only $\sim 40\%$ of all local Hα emitters have EW$_0 > 100$ Å (Gallego et al. 1997), and biases the search towards extremely late-type spiral, irregular and starburst galaxies (Kennicutt & Kent 1983). In the entire survey seven objects passed our selection thresholds, and their properties are listed in Table 2. Hα emission line fluxes and luminosities quoted in this table and elsewhere in this paper (but not in Table 1) have been corrected for a 25% contribution of the [N II] 6548+6584 Å system to the observed narrow-band flux excess (Kennicutt & Kent 1983). In calculating SFRs, we have used the empirical conversion factor derived by Kennicutt (1983), but not corrected for extinction.

The detections in our survey include three expected Hα emission line objects: the radio galaxies TX 0200+015 and TX 0211$-$122 and the object PHL 957–C1 (see Sect. 4.1.2). However, four additional Hα emitters were found with significances from 3 to 4. All of these lie at significant projected distances to the marker damped Lyα cloud or radio galaxy. The smallest projected distance is found for the object UM 196–G1, which lies at a projected proper distance of $60 \, h_{75}^{-1}$ kpc (for $q_0 = 0.1$) from the line of sight to the quasar. This distance is significantly larger than the typical radii of damped Lyα clouds, which are smaller than $30 \, h_{75}^{-1}$ kpc (Møller & Warren 1998), so that it is unlikely that any of the sources detected in the fields of damped Lyα systems in this survey are directly associated with the marker damped Lyα clouds. The properties of the detected sources and the implications of our survey are discussed in the next section. A sample color-magnitude diagram with significance curves and EW$_0$ limits, for one of the surveys fields is shown in Fig. 1. The parts of these fields containing the candidate emission line objects are shown in Figs. 2–7.

4. Discussion

4.1. Properties of individual fields and objects

4.1.1. The UM 196 field

The object G1 (Fig. 2) lies at a projected distance of $7.''7$ from the line-of-sight to the quasar, at a redshift consistent with the $z_{\mathrm{abs}} = 2.153$ damped Lyα system (Smith et al. 1986) towards this object. The object is spatially unresolved.

4.1.2. The PHL 957 field

The object PHL 957–C1 (Fig. 3) was initially discovered by Lowenthal et al. (1991) in a narrow-band Lyα survey. Its spectrum displays a narrow Lyα line, in addition to C IV 1549 Å and He II 1640 Å. While these lines may also be produced in high excitation H II regions and are detected in local starburst dwarf galaxies such as NGC 4214 (Leitherer et al. 1996) as well as in $z \sim 3$ Lyman break galaxies (LBGs; Steidel et al. 1996), they are much stronger in PHL 957–C1. Since in addition the absence of absorption lines suggests a non-stellar origin for the continuum, this object most likely harbours an active galactic

Table 2. Parameters of the detected emission line sources

object	$I_{H\alpha}$ [erg s^{-1} cm^{-2}]	$L_{H\alpha}$ [h_{75}^{-2} L$_\odot$]		SFR [h_{75}^{-2} M$_\odot$ yr^{-1}]		comments
		$q_0 = 0.1$	$q_0 = 0.5$	$q_0 = 0.1$	$q_0 = 0.5$	
UM 196–G1	$1.8 \cdot 10^{-16}$	$1.3 \cdot 10^9$	$6.7 \cdot 10^8$	44	23	a
PHL 957–C1	$2.8 \cdot 10^{-16}$	$2.6 \cdot 10^9$	$1.3 \cdot 10^9$	91	44	b,c
PHL 957–C2	$1.7 \cdot 10^{-16}$	$1.6 \cdot 10^9$	$7.8 \cdot 10^8$	54	26	a
PHL 957–C3	$1.9 \cdot 10^{-16}$	$1.8 \cdot 10^9$	$8.7 \cdot 10^8$	62	29	a
TX 0200+015	$6.1 \cdot 10^{-16}$	$5.1 \cdot 10^9$	$2.5 \cdot 10^9$	170	87	c
TX 0211−122	$6.6 \cdot 10^{-16}$	$6.0 \cdot 10^9$	$2.9 \cdot 10^9$	210	100	c
TX 0211−122–G1	$2.3 \cdot 10^{-16}$	$2.1 \cdot 10^9$	$1.0 \cdot 10^9$	73	35	a

[a] adopted redshift is redshift of the marker object
[b] previously detected in Lyα by Lowenthal et al. (1991)
[c] because of the active nucleus, SFR is an upper limit for this object
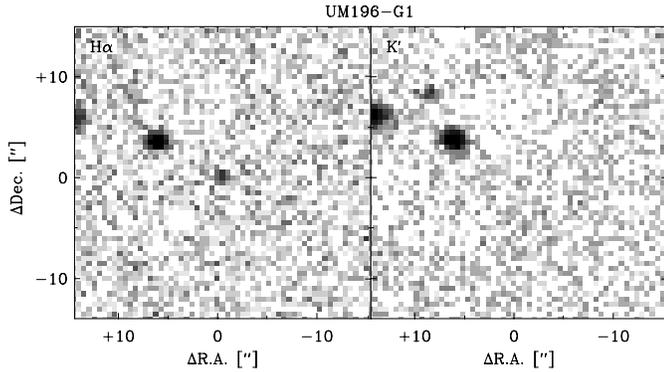

Fig. 2. Parts of the narrow-band redshifted Hα (left-hand panel) and broad-band K' (right-hand panel) frames showing in the centre the emission line object UM 196–G1. The brightest object in the images shown is the QSO UM 196.
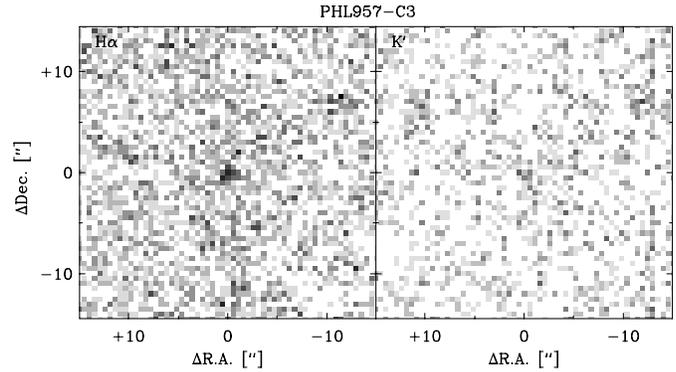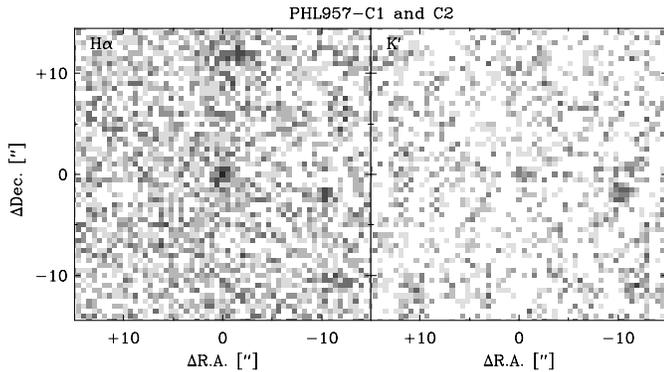

Fig. 3. Parts of the narrow-band redshifted Hα (left-hand panel) and broad-band K' (right-hand panel) frames showing in the centre the emission line object PHL 957–C1 and towards the North PHL 957–C2.
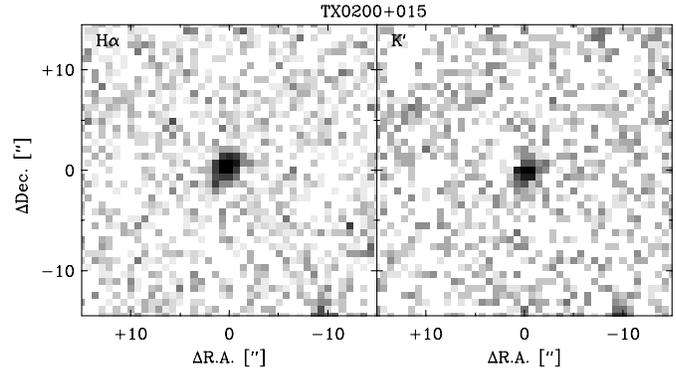

Fig. 4. Parts of the narrow-band redshifted Hα (left-hand panel) and broad-band K' (right-hand panel) frames showing in the centre the emission line object PHL 957–C3.

Fig. 5. Parts of the narrow-band redshifted Hα (left-hand panel) and broad-band K' (right-hand panel) frames containing in the centre the radio galaxy TX 0200+015.

nucleus (AGN). We therefore exclude this object from the discussion of starforming galaxies at $z \sim 2.2$ below. We note that this object was previously detected in Hα by Hu et al. (1993) and Bunker et al. (1995), with fluxes consistent with our result. The inferred ratio of Lyα/Hα is 2, which is well below the unattenuated case B recombination value of 8.10. The Hα image is

slightly elongated at a position angle of about $135°$. The object is located $48''$ from the line-of-sight to the QSO (360 kpc for $q_0 = 0.1$).

The objects C2 and C3 (Figs. 3 and 4) have not been detected before. They are located relatively close to C1, at distances of $12''.6$ and $18''.2$ (95 and 137 kpc for $q_0 = 0.1$) respectively. The upper limit on the Lyα emission from these objects given by
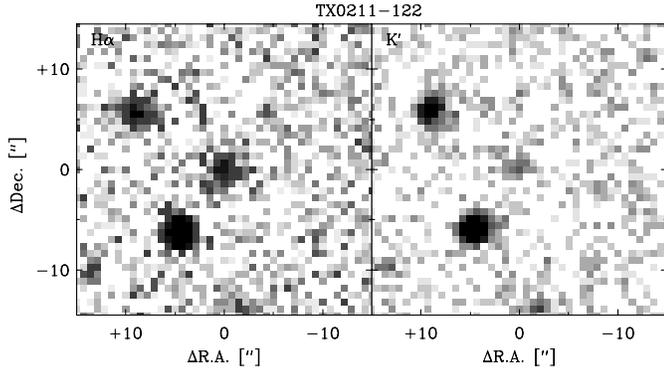
Fig. 6. Parts of the narrow-band redshifted Hα (left-hand panel) and broad-band K' (right-hand panel) frames containing in the centre the radio galaxy TX 0211$-$122.
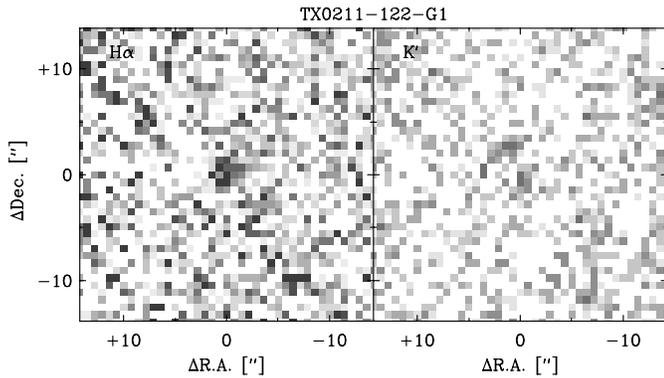

Fig. 7. Parts of the narrow-band redshifted Hα (left-hand panel) and broad-band K' (right-hand panel) frames containing the emission line object TX 0211$-$122–G1.

Lowenthal et al. (1991) implies Lyα/Hα ratios less than 0.085 and 0.095 respectively, showing that Lyα is strongly suppressed in these objects. The low emission line fluxes of these objects are consistent with their non-detection in Hα by Bunker et al. (1995).

Recently, Mannucci et al. (1998) have presented narrow-band imaging at $\lambda \approx 1.237$ μm of the field of PHL 957, which should contain the redhsifted [O II] 3727 Å emission from the Hα objects detected in our survey. Using the correlation between [O II] and Hα line strength derived by Kennicutt (1992), the expected [O II] line strengths of C1–C3 are consistent with their non-detection by Mannucci et al. (1998). Conversely, these authors report the detection of two emission line objects, which they interpret as [O II] emitters at the redshift of the damped Lyα system, so that the corresponding Hα emission should be detected in the present survey. Using the same correlation of [O II] and Hα as as above, these sources should produce Hα fluxes of $4.2 \cdot 10^{-16}$ and $5.9 \cdot 10^{-16}$ erg s^{-1} cm^{-2}, i.e., 7.4σ and 10.5σ detections in the present survey. However, these sources are not detected in our observations of this field, or in the earlier observations of the same field by Bunker et al. (1995), where these sources should also have been detected at high significance. It is very unlikely that an anomalously high [O II]/Hα ratio is the

origin of this discrepancy, since none of the galaxies in the extensive sample of Kennicutt (1992), which covers a wide variety of star forming and active galaxies, have a sufficiently high ratio. Another possibility is that the emission line objects detected in this field by Mannucci et al. (1998) are in fact due to Hα at $z = 0.88$, or perhaps [O III] 5007 Å at $z = 1.47$, or, more prosaically, that they are spurious objects (note that the authors do not assign high significances to these objects).

4.1.3. The TX 0200+015 field

Our Hα image of the $z = 2.230$ radio galaxy TX 0200+015 (Fig. 5) reveals an elongated emission region at a position angle agreeing very well with the position angle of $155°$ of the radio jet (Röttgering et al. 1994). The two radio lobes are only $5\overset{''}{.}1$ apart and the Hα emission fills most of the space between the lobes. The continuum is extended along the same position angle, but is more centrally concentrated. The Hα+[N II] flux of $8.1 \cdot 10^{-16}$ erg s^{-1} cm^{-2} that we detect is more than a factor of 2 below the spectroscopic value by Evans (1998). Given the high S/N of his spectrum, combined with the fact that the lines are very well centred in the narrow-band filter used in the present survey, the difference is significant and probably indicates the presence of extended low surface brightness emission below the detection limit of our image; the presence of such emission is indeed indicated by the long slit Lyα spectrum presented by Van Ojik et al. (1997). For an Hα/[N II] ratio of unity, which is a typical value for radio galaxies as shown by the survey by Eales & Rawlings (1993), the implied Lyα/Hα ratio is 1.7, far below the case B recombination value and also lower than commonly found values in high redshift radio galaxies (e.g., McCarthy et al. 1992). Evans (1998) estimates that the Hα+[N II] complex accounts for $28\pm2\%$ of the broad-band K flux. However, the line emission is not sufficiently bright to account for the elongation in the K' image (Fig. 5), so that the alignment between radio and (rest-frame) optical emission in this radio galaxy is present in Hα as well as in the underlying continuum.

4.1.4. The TX 0211$-$122 field

The $z = 2.338$ radio galaxy TX 0211$-$122 (Fig. 6) was studied in some detail by Van Ojik et al. (1994) who discussed its peculiar spectrum which shows a strongly suppressed Lyα line. A high resolution spectrum (Van Ojik et al. 1997) revealed prominent Lyα absorption features superposed on the emission line. Assuming again an Hα/[N II] ratio of unity, and using the Lyα flux from Röttgering et al. (1997) we obtain a Lyα/Hα ratio of only 1.3, far below the case B recombination value. The Hα+[N II] complex accounts for 11% of the broad-band K' flux density. The K' image shows a slightly extended object, at a position angle agreeing very well with the radio position angle of $102°$ (Röttgering et al. 1994). The continuum morphology is in agreement with the morphology seen in HST WFPC2 imaging by Pentericci et al. (1999). The Hα image on the other hand is more extended, shows diffuse emission around the radio galaxy,

and an extension or second component at position angle $135°$, substantially deviating from the radio axis.

The emission line object G1 Fig. 7 lies at a projected distance of $80''9$ (0.6 Mpc projected proper distance for $q_0 = 0.1$) from the radio galaxy. This object has a complex morphology, showing two continuum components. The Hα emission is located between the two continuum components, slightly closer to the South-West component. This object may be an example of a high-redshift merger, which is consistent with its high inferred SFR.

4.1.5. The Q0000$-$2619 field

The field of Q0000$-$2619 contains a damped Lyα system at $z = 3.390$ (first described by Schneider et al. 1989). The absorbing galaxy is located close to the line-of-sight to the QSO and is at $z = 3.408$ (Steidel & Hamilton 1992). An additional galaxy at $z = 3.428$ has been found through narrow-band Lyα imaging (Macchetto et al. 1993; Giavalisco et al. 1994). [O III] 5007 Å emission from these objects could have appeared in our narrow-band images of this field, but no line emitters were found to a 3σ upper limit of $4.8 \cdot 10^{-16}$ erg s^{-1} cm^{-2}. We therefore chose to treat this field as an untargeted survey for Hα emission at $z \sim 2.39$.

4.2. Survey limits and their implications

The limits implied by our survey are presented in Fig. 8, in terms of a comoving number density of galaxies as a function of Hα flux or of total SFR. We have excluded the two radio galaxies and the object PHL 957–C1 from this analysis, since an unknown fraction of their Hα emission may be powered by an AGN rather than star formation. The comoving volume density limits represent 90% confidence levels based on Poisson statistics (Gehrels 1986). Hα luminosity and SFR limits denote 3σ levels. For comparison, we have also included the limits provided by the deepest narrow-band survey to date (the Keck survey by Pahre & Djorgovski 1995) and by the widest survey to date, by Thompson et al. (1995). The limits of these surveys have been recalculated by us considering *only* Hα at $z = 2.1$–2.4. It should be noted that all of these surveys are also sensitive to other emission lines (e.g., [O II] 3727 Å, [O III] 5007 Å). This property has often been used to artificially increase the survey volumes by simultaneously considering a number of lines, assuming fixed ratios of these lines to Hα (Mannucci & Beckwith 1995). However, we emphasize that this procedure is fraught with considerable uncertainties, since ratios of e.g., [O III] 5007 Å to Hα in local galaxies cover a large range of values (Kennicutt 1992), and depend strongly on excitation and abundance effects. The [O II]/Hα ratio, which is, in comparison to other line ratios, relatively well-behaved in local galaxies, still varies by factors of typically up to 5, and occasionally more (Kennicutt 1992). More fundamentally, limits based on a narrow-band image at a fixed wavelength, but calculated by considering *simultaneously* a number of lines at different wavelengths that could appear in the narrow-band frame at different redshifts (as has been done

for some of the previous surveys), completely destroy any information on the redshift dependence of the SFD. The result is a complicated weighted average value over a number of redshifts, and very difficult to interpret. It is therefore strongly preferable to calculate limits pertaining to only fairly narrow redshift intervals, based on a single emission line, providing a reliable measure of the SFR. Following this reasoning we note that in principle our survey could also be used for obtaining a limit on the SFD at $z = 4.5$–5.0, since it is sensitive to [O II] 3727 Å in that redshift interval. However, since the resulting limit is not very constraining, we do not present that analysis here, and limit ourselves to considering Hα emission, since (as will be shown in Sect. 4.3.1), this is by far the most likely emission line identification.

The (non-AGN) emission-line objects found in the present survey have extinction-corrected SFRs from 44 to $73\,h_{75}^{-2}$ M$_\odot$ yr^{-1} for $q_0 = 0.1$ and of 23 to $35\,h_{75}^{-2}$ M$_\odot$ yr^{-1} for $q_0 = 0.5$. Locally, such SFRs are found in starburst galaxies. In Fig. 8 we also compare available survey limits to the local extinction-corrected Hα luminosity function (Gallego et al. 1995) and evolved versions of this function, using simple translational backward evolution models. Since both Hα and far-IR emission are proportional to SFR, it is reasonable to assume similar evolution laws for the Hα and far-IR luminosity functions. The evolution of the far-IR luminosity function, reviewed by Rowan-Robinson (1996), can be described as proportional to $(1 + z)^\alpha$, with $\alpha \approx 3$ for pure luminosity evolution, or $\alpha \approx 5.8$ for pure density evolution. The local Hα luminosity function, evolved according to these evolutionary scenarios, is plotted in Fig. 8, where we have continued the evolution backward to a redshift z_e. Inspection of Fig. 8 suggests that some detections would be expected in the combined surveys for pure luminosity evolution to $z_e = 2$, but none in the other cases considered.

4.3. Implications for star formation at $z = 2.25$

4.3.1. Contamination

Our sample of $z = 2.1$–2.4 star forming galaxies may be contaminated by interlopers at different redshifts, and by AGNs misidentified as starburst galaxies.

As far as interlopers at different redshifts are concerned, only four emission lines may contaminate our sample: [O II] 3727 Å at $z = 4.5$–5.0, Hβ 4861 Å at $z = 3.2$–3.6, [O III] 5007 Å at $z = 3.1$–3.5 and Paα 1.875 μm at $z = 0.1$–0.2. Other emission lines are too faint to cause a potential problem. Interlopers due to Paα occur only at such low redshifts that, at the magnitude levels involved, extended emission should have been detected. Furthermore, the implied Paα rest-frame equivalent widths would be so large that extremely young starburst galaxies (ages less than a few million years) with essentially no contribution from an older population to the continuum (even at 1.9 μm rest wavelength) would be implied (Leitherer & Heckman 1995), a very unlikely result.

As for the other lines, if the narrow-band excess emission would in fact be Hβ, [O III] or [O II], the objects would be at
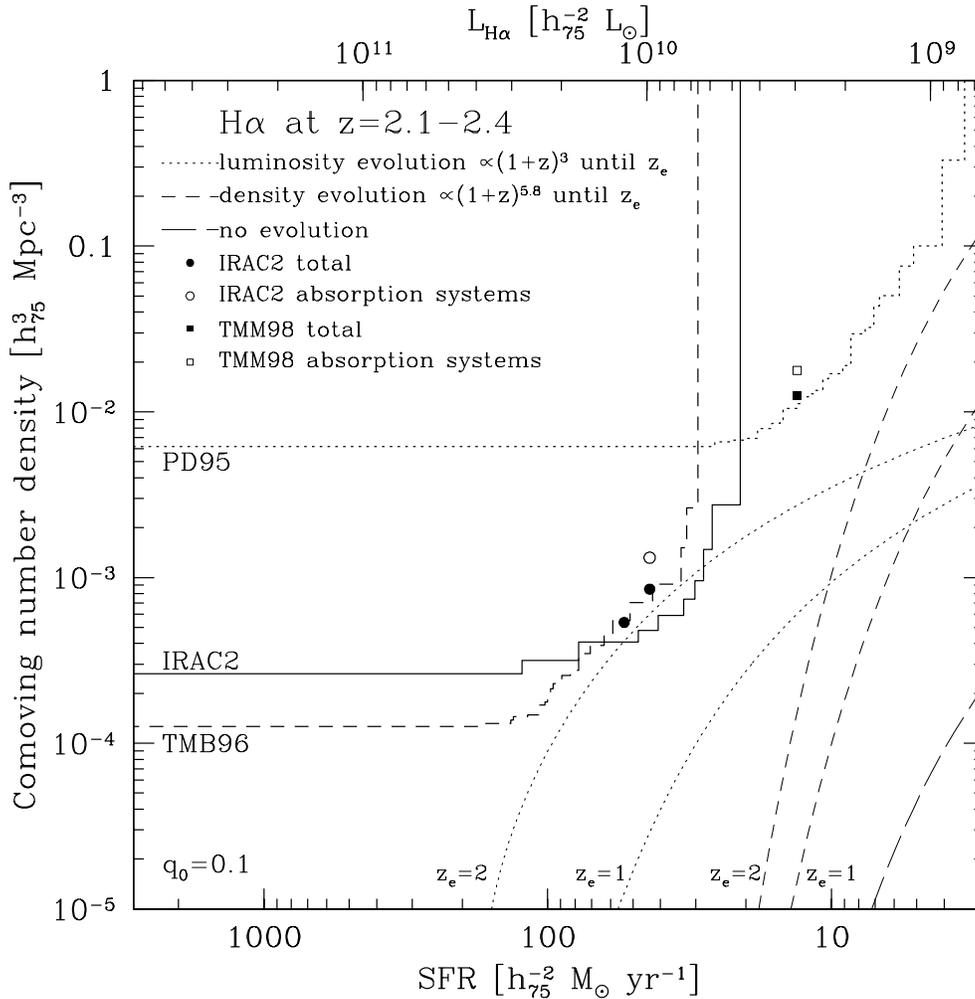
Fig. 8. Limits of the present survey (labeled "IRAC2") expressed as limiting comoving volume density at the 90% confidence level (vertical axis) as a function of Hα luminosity (top horizontal axis) or total SFR (bottom horizontal axis). Details of the derivation of SFRs and comoving density limits are given in Sects. 3 and 4.2. For comparison, the results of Pahre & Djorgovski (1995) and Thompson et al. (1996), (labeled "PD95" and "TMB96" respectively) are also shown. The filled circles represent the non-AGN emission line objects detected in the present survey (IRAC2), while the filled square (TMM98) represents the survey by Teplitz et al. (1998). Open symbols represent these same surveys considering only fields targeted at absorption line systems. The PD95, TMB96 and TMM98 results have been converted to correspond to the same cosmology and conversion to SFR as used in the present paper. The long-dashed curve represents the *cumulative* local (extinction-corrected) Hα luminosity function (i.e., the comoving volume density of galaxies with an intrinsic Hα luminosity higher than the value indicated on the top horizontal axis) of Gallego et al. (1995). The dotted curves show this cumulative luminosity function after applying pure luminosity evolution proportional to $(1 + z)^3$ ending at a redshift z_e. Similarly, the short-dashed curves are based on the local Hα luminosity function assuming pure density evolution proportional to $(1 + z)^{5.8}$ ending at redshift z_e. Evolutionary calculations for both $z_e = 1$ and $z_e = 2$ are shown.

much higher redshift and intrinsically much more luminous than in the case of Hα, implying much more extreme results. Therefore, identification with [O III] or [O II], although not ruled out, is *a priori* much less likely than with Hα, and identification with Hα is in this sense a conservative approach. We note that it is a general property of near-IR Hα surveys that interlopers due to other bright optical lines are unlikely, in contrast to optical surveys for Lyα emission where interlopers are frequent (e.g., Thompson & Djorgovski 1995). We thus conclude that contamination due to other emission lines is unlikely.

Since our survey redshift interval lies at the peak of the "AGN era" where the comoving number density of AGNs has

a maximum (e.g., Shaver et al. 1996; Boyle & Terlevich 1998), the possibility that the Hα emission of some of our detected objects is powered by AGNs rather than by star formation must be considered. In the absence of additional information, we can only use statistical arguments. Locally, the spectroscopic survey results by Gallego et al. (1997) imply that at most 5% of Hα-selected galaxies contain AGNs. For rest-frame Hα equivalent widths $EW_0 > 100$ Å, as for our sources, the fraction of AGNs is higher, but still very much smaller than that of non-AGNs. Evidence that the fraction of AGNs among Hα-selected galaxies does not greatly increase with z, is provided by the sample of $z > 2$ Hα emitters of Teplitz et al. (1998), who find only two

AGNs in a sample of thirteen Hα emitters. Alternatively, we may use the luminosity function of $z > 2$ quasars (Warren et al. 1994) to estimate the comoving number density of AGNs of the magnitude observed here at $z = 2.25$, using a large extrapolation downward in magnitude, since our detections are much fainter than typical quasars. This procedure yields an expected space density of AGNs at the relevant magnitudes which is one to two orders of magnitude smaller than that of the Hα emitters found in our survey. Hence it is unlikely that our sample is significantly contaminated by AGNs.

It is obvious that only follow-up spectroscopy can give definitive answers on the presence of AGNs and on the (un)importance of interlopers at different redshifts, and is a necessary step once more extensive samples are collected. The general arguments given above indicate however, that there is no problem of contamination for our very small number of objects.

4.3.2. Effects of field selection

For $q_0 = 0.1$, the comoving density of non-AGN emission line sources in our survey is approximately $1 \cdot 10^{-3} h_{75}^3$ Mpc^{-3} for objects with $\dot{M}_* \geq 44$ M$_\odot$ yr^{-1}. This density is similar to the density of $z \sim 3.0$–3.5 LBGs as determined by Steidel et al. (1996) and of Hα emitters at $z = 0.7$–1.9 found in the NICMOS grism survey (McCarthy et al. 1999); however, taking into account the different assumptions on conversion to SFR (see Van der Werf 1997 for a summary) and cosmological parameters, the LBGs and the NICMOS grism survey galaxies have significantly lower implied SFRs. This result suggests an enhanced source density in the present survey, most likely as a result from the fact that our survey is targeted at "marker" objects and not a blank field survey. It is therefore necessary to assess the effect of these "marker" objects on our source detection rate.

It is noteworthy that 75% of our detected emission line objects are found in fields targeted at damped Lyα systems. Only one object is found in fields targeted at radio galaxies, and the untargeted fields do not contain any emission line candidates. The high success rate for damped Lyα fields is consistent with earlier reports by Mannucci et al. (1998) who found 12 objects at $z = 2.3$–2.4 (and 6 at $z = 0.89$) in a survey targeted at damped Lyα and strong metal absorber redshifts, to an area-weighted flux limit of $2.4 \cdot 10^{-16}$ erg s^{-1} cm^{-2}, comparable to the depth of the present survey. In contrast, the survey by Thompson et al. (1996), which was only slightly less deep (flux limit $3.5 \cdot 10^{-16}$ erg s^{-1} cm^{-2}) but which was targeted at quasar redshifts, yielded in a much larger area only one emission line candidate (Thompson et al. 1996), subsequently spectroscopically confirmed by Beckwith et al. (1998). A deeper survey (3σ flux limit $7 \cdot 10^{-17}$ erg s^{-1} cm^{-2}) by Teplitz et al. (1998) produced a qualitatively similar result: thirteen Hα emitters were detected (two of which are AGNs) in an $11\square'$ survey; twelve of the thirteen candidates were found in fields targeting absorption line systems, only one is associated with a quasar. Taking into account the volumes surveyed, the implied source density associated with absorption line systems is at least 4 times higher than

in fields targeting quasar redshifts. A high success rate of detecting Hα emitters associated with damped Lyα systems has also been reported by Bechtold et al. (1998). This point is further illustrated in Fig. 8 where the detections in the present survey and in the survey by Teplitz et al. (1998) are shown, both for the total surveys and only for fields targeted at absorption line systems; the latter procedure consistently produces a higher source density. All of the surveys referred to above produce similar source densities (at the flux densities probed here) to the present survey, if only fields targeting absorption systems are considered, and thus corroborate the results of the present survey. These results thus point towards a much higher density of star forming galaxies associated with absorption line systems than in other targeted (or untargeted) surveys. Therefore, surveys targeting absorption systems cannot be used to derive a cosmic SFD, but will only provide an upper limit. This upper limit can be quantified by considering only the detections in damped Lyα fields in the present survey and in the survey by Teplitz et al. (1998), which yields an SFD of approximately $\dot{\rho}_* \sim 0.2 h_{75}$ M$_\odot$ yr^{-1} Mpc^{-3}. In terms of a *metal production density* (MPD) $\dot{\rho}_Z$, which is much less sensitive to assumptions on the IMF (Madau et al. 1996), the value $\dot{\rho}_Z \sim 2 \cdot 10^{-3} h_{75}$ M$_\odot$ yr^{-1} Mpc^{-3} results. A more accurate analysis should consider the total luminosity function of star forming galaxies in our survey volumes, but our sample if far too small for deriving a luminosity function. In order to esimate the order of magnitude of the error involved in only considering detected galaxies, we note that, using a faint-end slope $\alpha = -1.3$ as for the local Hα field luminosity function (Gallego et al. 1995), a Schechter function with SFR$^* \sim 35 h_{75}$ M$_\odot$ yr^{-1} and $\phi^* = 0.02 h_{75}^3$ Mpc^{-3} would adequately represent our results, and this would result in about 40% higher estimates for the SFD and MPD. These values exceed SFDs and MPDs determined from rest-frame UV data (even after these have been corrected for extinction) by factors of typically 2 to 5 (Steidel et al. 1999). This discrepancy underlines the fact that fields targeted at absorption systems probe overdense regions, and surveys in such fields cannot be used to determine a globally valid cosmic SFD.

5. Conclusions and outlook

We have presented results from a large-area survey for Hα emission at $z = 2.1$–2.4, using a combination of deep narrow-band and broad-band imaging in the near-IR K-band. With a total comoving volume of $8.8 \cdot 10^3 h_{75}^{-3}$ Mpc^3 (for $q_0 = 0.1$), our survey covers almost 50% of the comoving volume of the most extensive comparable published survey to date, but goes considerably deeper. Four emission line objects are serendipitously detected in our survey, with inferred star formation rates of 44 to $73 h_{75}^{-2}$ M$_\odot$ yr^{-1}. Statistical arguments indicate that these objects are star forming galaxies, and that contamination of our sample with AGNs is highly unlikely. The results from this survey and other surveys show that the space density of star forming galaxies at $z = 2.1$–2.4 associated with absorption line systems is significantly higher than that in the vicinity of known radio galaxies or quasars and in the general field. As a result, a lumi-

nosity function consistent with these surveys can only provide an upper limit to the cosmic star formation density at these redshifts.

This result shows that narrow-band/broad-band Hα surveys in the near-IR are feasible and begin to give interesting results. Future surveys using large-format near-IR arrays on 4–8 m class telescopes will be able to probe much fainter luminosities, while covering larger areas. Most importantly, with such instrumentation untargeted surveys will become feasible, which, as we have shown in Sect. 4.3.2, is necessary in order to use these surveys for estimating a cosmic SFD. In order to avoid the biases resulting from targeted surveys as described in the present paper, a larger area and considerably deeper *untargeted* field survey has recently been conducted with the SOFI near-infrared camera at the ESO New Technology Telescope, using the same narrow-band/broad-band technique as described above. Several sources have been detected and spectroscopically confirmed. A preliminary analysis is presented by Moorwood et al. (2000) and indeed yields a lower density than in fields targeted at absorption line systems. A more detailed analysis and paper is in preparation. This project demonstrates the feasibility of untargeted surveys for Hα emission at $z \sim 2.2$ using the narrow-band/broad-band technique described here. By carrying out such a survey at a number of discrete redshifts out to $z = 2.2$, the evolution of the Hα luminosity function and of the metal production and star formation density can be studied over the crucial redshift range where these densities reach their maximum values. Such projects will be of great importance for our understanding of galaxy evolution since $z = 2.5$.

References

Afonso J., Cram L., Mobasher B., 2000, ApJ 536, 68

Bechtold J., Elston R., Yee H.K.C., Ellingson E., Cutri R.M., 1998, In: D'Odorico S., Fontana A., Giallongo E. (eds.) The young universe: galaxy formation and evolution at intermediate and high redshift. ASP Conference Series 146, p. 241

Beckwith S.W.V., Thompson D., Mannucci F., Djorgovski S.G., 1998, ApJ 504, 107

Bertin E., Arnouts S., 1996, A&AS 117, 393

Blain A.W., Smail I., Ivison R.J., Kneib J.P., 1999, MNRAS 303, 423

Boyle B.J., Terlevich R.J., 1998, MNRAS 293, L49

Bunker A.J., Warren S.J., Hewett P.C., Clements D.L., 1995, MNRAS 273, 513

Cardelli J.A., Clayton G.C., Mathis J.S., 1989, ApJ 345, 245

Charlot S., Fall S.M., 1991, ApJ 378, 471

Charlot S., Fall S.M., 1993, ApJ 415, 580

Charlot S., 1999, In: Benvenuti P. (ed.) NGST - Science drivers and technological challenges. ESA-SP 429, European Space Agency, Paris, p. 135

Chen W.L., Neufeld D.A., 1994, ApJ 432, 567

Collins C.A., Parkes I.M., Joseph R.D., 1996, MNRAS 282, 903

Cowie L.L., Hu E.M., 1998, ApJ 115, 1319

Devillard N., Jung Y., Cuby J.G., 1999, The Messenger 95, 5

Djorgovski S., 1992, In: De Carvalho R.R. (ed.) Cosmology and large-scale structure in the universe. ASP Conf. Series 24, p. 73

Eales S.A., Rawlings S., 1993, ApJ 411, 67

Evans A.S., 1998, ApJ 498, 553

Gallego J., Zamorano J., Aragón-Salamanca A., Rego M., 1995, ApJ 455, L1

Gallego J., Zamorano J., Rego M., Vitores A.G., 1997, ApJ 475, 502

Gehrels N., 1986, ApJ 303, 336

Giavalisco M., Macchetto F.D., Sparks W.B., 1994, A&A 288, 103

Glazebrook K., Blake C., Economou F., Lilly S., Colless M., 1999, MNRAS 306, 843

Howell S.B., 1989, PASP 101, 616

Hu E.M., McMahon R.G., 1996, Nat 382, 281

Hu E.M., Songaila A., Cowie L.L., Hodapp K.W., 1993, ApJ 419, L13

Hu E.M., Cowie L.L., McMahon R.G., 1998, ApJ 502, L99

Hughes D.H., Serjeant S., Dunlop J., et al., 1998, Nat 394, 241

Kennicutt R.C., Kent S.M., 1983, AJ 88, 1094

Kennicutt R.C., 1983, ApJ 272, 54

Kennicutt R.C., 1992, ApJ 388, 310

Leitherer C., Heckman T.M., 1995, ApJS 96, 9

Leitherer C., Vacca W.D., Conti P.S., et al., 1996, ApJ 465, 717

Lilly S.J., Lefèvre O., Hammer F., Crampton D., 1996, ApJ 460, L1

Lowenthal J.D., Hogan C.J., Green R.F., et al., 1991, ApJ 377, L73

Macchetto F., Lipari S., Giavalisco M., Turnshek D.A., Sparks W.B., 1993, ApJ 404, 511

Madau P., Henry C. Ferguson, Dickinson M.E., et al., 1996, MNRAS 283, 1388

Mannucci F., Beckwith S.V.W., 1995, ApJ 442, 569

Mannucci F., Thompson D., Beckwith S.V.W., Williger G.M., 1998, ApJ 501, L11

McCarthy P.J., Elston R., Eisenhardt P., 1992, ApJ 387, L29

McCarthy P.J., Yan L., Freudling W., et al., 1999, ApJ, in press

Meurer G.R., Heckman T.M., Calzetti D., 1999, ApJ 521, 64

Møller P., Warren S.J., 1998, MNRAS 299, 661

Moorwood A.F.M., Finger G., Biereichel P., et al., 1992, The Messenger 69, 61

Moorwood A.F.M., Van der Werf P.P., Cuby J.G., Oliva E., 2000, to appear in: Lutz D., Tacconi L. (eds.) Ultraluminous galaxies: babies or monsters

Pahre M.A., Djorgovski S.G., 1995, ApJ 449, L1

Pentericci L., Röttgering H.J.A., Miley G.K., et al., 1999, A&A 341, 329

Pettini M., Kellogg M., Steidel C.C., et al., 1998, ApJ 508, 539

Röttgering H.J.A., Lacy M., Miley G.K., Chambers K.C., Saunders R., 1994, A&AS 108, 79

Röttgering H.J.A., Van Ojik R., Miley G.K., et al., 1997, A&A 326, 505

Rowan-Robinson M., 1996, In: Bremer M.N., Van der Werf P.P., Röttgering H.J.A., Carilli C.L. (eds.) Cold gas at high redshift. Kluwer, Dordrecht, p. 61

Schneider D.P., Schmidt M., Gunn J.E., 1989, AJ 98, 1507

Shaver P.A., Wall J.V., Kellermann K.I., Jackson C.A., Hawkins M.R.S., 1996, Nat 384, 439

Smith H.E., Cohen R.D., Bradley S.E., 1986, ApJ 310, 583

Steidel C.C., Hamilton D., 1992, AJ 104, 941

Steidel C.C., Giavalisco M., Pettini M., Dickinson M., Adelberger K.L., 1996, ApJ 462, L17

Steidel C.C., Adelberger K.L., Giavalisco M., Dickinson M., Pettini M., 1999, ApJ, in press

Teplitz H.I., Malkan M., McLean I.S., 1998, ApJ 506, 519

Thompson D., Djorgovski S.G., 1995, AJ 110, 982

Thompson D., Djorgovski S., Beckwith S.V.W., 1994, AJ 107, 1

Thompson D., Djorgovski S., Trauger J., 1995, AJ 110, 963

Thompson D., Mannucci F., Beckwith S.V.W., 1996, AJ 112, 1794

Van der Werf P.P., 1997, In: Mamon G.A., Thuân T.X., Vân J.T.T. (eds.) Extragalactic astronomy in the infrared. Editions Frontières, Paris, p. 451

Van Ojik R., Röttgering H.J.A., Miley G.K., et al., 1994, A&A 289, 54

Van Ojik R., Röttgering H.J.A., Miley G.K., Hunstead R.W., 1997, A&A 317, 358

Wainscoat R.J., Cowie L.L., 1992, AJ 103, 332

Warren S.J., Hewett P.C., Osmer P.S., 1994, ApJ 421, 412